Solar Energy Materials & Solar Cells 98 (2012) 216–223

Contents lists available at SciVerse ScienceDirect

Solar Energy Materials & Solar Cells

journal homepage: www.elsevier.com/locate/solmat

Crack detection in photovoltaic cells by interferometric analysis of electronic speckle patterns

Tzu-Kuei Wen, Ching-Chung Yin*

Department of Mechanical Engineering, National Chiao Tung University, 1001, Ta Hsueh Road, Hsinchu 30010, Taiwan, Republic of China

ARTICLE INFO

Article history:
Received 28 July 2011
Accepted 29 October 2011
Available online 22 November 2011

Keywords:
Crack detection
Electronic speckle pattern interferometry
Photovoltaic cell
Crystalline silicon

ABSTRACT

Cracking is a common problem encountered during the fabrication of crystalline silicon photovoltaic (PV) cells. In this study, electronic speckle pattern interferometry (ESPI) is developed as a tool for rapid identification of cracks in PV cells. Thermally induced cell deformation of defect-free and defect-bearing PV cells was first modeled with numerical simulations and then experimentally studied by optical configuration for ESPI measurement of out-of-plane deformations. Both numerical and experimental results indicate that the speckle patterns imparted during thermal deformation of a cell allow for simultaneous quantification of crack size, location and type in both single- and poly-crystalline PV cells. Speckle patterns near defects were manifested as continuous, chevron-shaped, and broken fringes for scratch, surface cracks, and through cracks, respectively. For comparison to other existing techniques, full field electroluminescent images were also provided for every defective PV cell. Electroluminescent imaging is capable of detecting cracks, but unlike ESPI, is unable to distinguish between the different types of cracks. Because the amount of heating needed to induce out-of-plane deformation resolvable by ESPI is small ($<0.5\ ^{\circ}C$) and because ESPI is sensitive to crack type, the ESPI-based imaging study presented here can potentially be developed into a rapid, non-destructive inspection tool for the structural integrity of solar cells at any point within the manufacturing process.

1. Introduction

The photovoltaic (PV) industry has rapidly developed new technologies in recent years. Crystalline silicon, and particularly polycrystalline silicon, is now used in 80–90% of PV cells produced worldwide. Crystalline silicon cells are expected to remain the dominant technology in the PV industry for at least the next decade due to their high current average efficiency and excellent stability. Manufacturers of PV cells and modules tend to focus on electrical performance rather than on mechanical strength. However, manufacturing flaws are common in crystalline silicon PV cells, particularly those that require several fabrication steps. Although the new manufacturing procedures enable production of silicon wafers thinner than 120 μm, which provides good flexibility [1], crystalline silicon PV cells remain hard and brittle in thickness near 200 μm. Photovoltaic cells and systems must be capable of operating in harsh environments when the thickness is reduced. Unexpected cracking not only reduces yield but is a major cause of catastrophic failure during production and operation. Assessing solar cell integrity before or during module processing is therefore essential for minimizing production costs.

Most mechanical defects in thin PV cells are surface cracks initiated from scratches during fabrication. It has previously been shown that the lowest strain energy release rate required for crack growth in single crystal silicon occurs in the {111} plane [2]. In an X-cut single-crystalline silicon wafer, crack propagation takes place along the ⟨110⟩ direction with cleavage plane inclined to the wafer plane. In polycrystalline wafers, however, the crack propagation is irregular and tends to zigzag. In both polycrystalline and single-crystalline solar cells, crack propagation in the depth direction typically terminates or is strongly reduced at the interface between the silicon layer and the porous Al contact back layer because an Al–Si eutectic layer, with a high fracture toughness [3,4], is generated at this interface during contact-firing. An example of a surface crack in a crystalline silicon PV cell is shown in Fig. 1. However, crack propagation can be enhanced if the cell undergoes bowing or flexing. Cell-bowing is a common problem related to the mismatch of thermal expansion coefficients between the Si layer and Al back contact layer, and as a consequence, cell-bowing can occur during the contact-firing fabrication process as well as during operation because solar cells are subjected to strong diurnal-nocturnal variations in temperature [5]. The generation of strong thermal stresses within the solar cell could promote crack branching and even propagation through the Al–Si eutectic layer, generating a through crack. While cell-bowing is generally easy to identify

* Corresponding author. Tel.: +886 3 5718965; fax: +886 3 5720634.
E-mail address: ccyin@faculty.nctu.edu.tw (C.-C. Yin).

0927-0248/$ - see front matter © 2011 Elsevier B.V. All rights reserved.
doi:10.1016/j.solmat.2011.10.034

using common optical procedures, the depth-extent of the cracks is not so easily detected.

Because the quality of solar cells can be seriously fractured by hairline cracks, the PV industry requires a fast and precise on-line method of crack detection and characterization. Instead of visual inspection, which is time-consuming and often overlooks very thin cracks, various techniques and approaches have been used to detect defects in silicon wafers and PV cells. Electroluminescence (EL) [6,7] and photoluminescence (PL) [8] imaging have been used to detect defects by taking advantages of the fact that electrical performance is reduced at defects, thereby reducing luminescence efficiency. Although those luminescence methods can detect fractures, they cannot clearly distinguish between surface scratches and cracks. Another imaging method is illuminated lock-in thermography [9,10], in which heat radiation from a sample is imaged by an infrared camera. However, even though this approach obtains high resolution imaging of defects, the lock-in integration needed to improve signal-to-noise ratio is extremely time consuming. Yet another method is resonance ultrasonic vibrations (RUV) [11], wherein silicon wafer quality is assessed using changes in the resonant frequency and bandwidth of the sample. This method, however, is only sensitive to bulk properties and cannot be used to identify crack density or geometry. In summary, each of these inspection methods has specific advantages in the individual manufacturing process of solar cells. None of these methods provides both rapid and detailed information on crack type and geometry.

An alternative approach is electronic speckle pattern interfermoetry (ESPI), which is an effective non-contact method of measuring deformation based on correlation of speckle interference patterns produced by real-time subtraction of sequential speckle images captured before and after an imposed deformation. Unlike traditional holographic interferometry, the interferometric fringe patterns of ESPI are recorded by CCD camera, which eliminates time-consuming chemical development and therefore speeds up the process. ESPI has been used for measuring thermal deformation in small electronic power devices [12] and large structural components [13] as well as for nondestructive inspection of cracks on metal plates [14].

This paper presents a method of rapidly detecting cracks in PV cells with ESPI to measure out-of-plane deformation induced by small thermal perturbations. The method relies on variation of strain distribution due to thermal deformation in the solar cell caused by discontinuities in material properties or the crystal lattice. The former is related to differences in thermal expansion coefficients between the Si layer and Al back contact layer while the latter is imparted by defects, such as cracks. In defect-free sample, the deflection of the cell due to mismatch in material properties of the Si and Al layers represents the background strain distribution. However, in the presence of cracks, the strain field becomes strongly localized. For example, the stress field around crack tips will be manifested in mixed modes [15], resulting in in-plane and out-of-plane perturbations to the background strain field. The out-of-plane displacement field is of interest in this study because cracks exhibit larger deformation caused by bending than by tension in a thin plate. ESPI should in theory be highly sensitive to small out-of-plane displacements, and the presence of cracks should be manifested in the form of discontinuous displacement fields, which would be evident in the shape and continuity of interference patterns. Below, we first perform numerical models to test the feasibility of this method. We then verify this method by performing actual experiments on solar cells. We also compare the ESPI approach to that of EL to assess whether this method may be a more effective inspection tool for structural defects in PV cells.

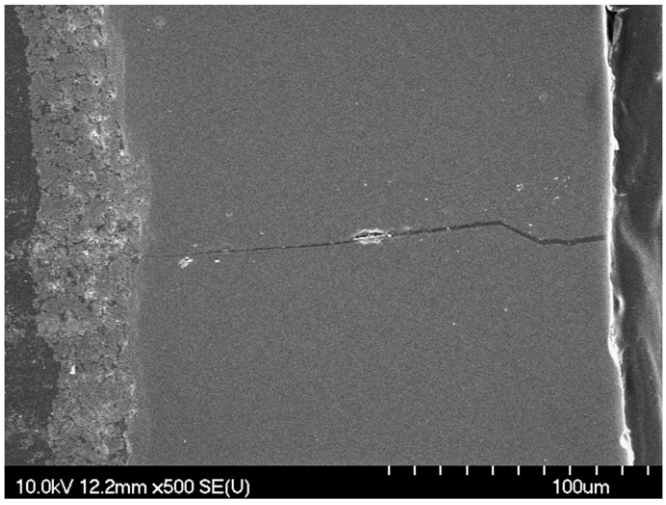

Fig. 1. SEM image of a surface crack in cross-sectional view within crystalline silicon PV. Surface is shown on the right. Al–Si eutectic layer is shown on the left. Crack appears to have initiated at the surface and propagated into the Si layer, but terminates at the Al–Si eutectic layer.

2. Feasibility tests using FEA models

We carried out a feasibility study of ESPI inspection for various defects in PV cells using numerical models based on a commercial finite element analysis (FEA) code ANSYS 13.0 (ANSYS Inc., Canonsburg, PA, USA). The models assume polycrystalline silicon cells with the dimension $156 \times 156 \times 0.2$ mm and single crystalline silicon solar cells with similar dimensions but with the corner reduction up to 15×15 mm. Each PV cell model contains silicon of 170 μm thickness, an aluminum back contact layer of 30 μm thickness and regular metal contacts (gridlines and busbars). Table 1 lists the material properties used in the calculation [16–18]. The displacement field around a flaw is of greater interest than stress distribution near the crack tip in this study. We adopted the 8-node isoparametric solid elements SOLID45 in ANSYS instead of crack elements at the crack tip in computation. The meshed model is composed of at least 3 elements in the

Table 1
Material properties used for calculation.

	Elastic modulus (GPa)		Density (g/cm^3)	Poisson's ratio	CTE (ppm/K)
Polysilicon	160		2.33	0.28	2.6
Single silicon	E_x=169,	G_{yz}=79.6	2.33	v_{yz}=0.36	3.6
	E_y=169,	G_{zx}=79.6		v_{zx}=0.28	
	E_z=130,	G_{xy}=50.9		v_{xy}=0.064	
Gridline and busbar (Ag)	72		10.5	0.28	18.9
Al layer	43		2.7	0.35	3.7 for poly-Si 5.5 for single Si

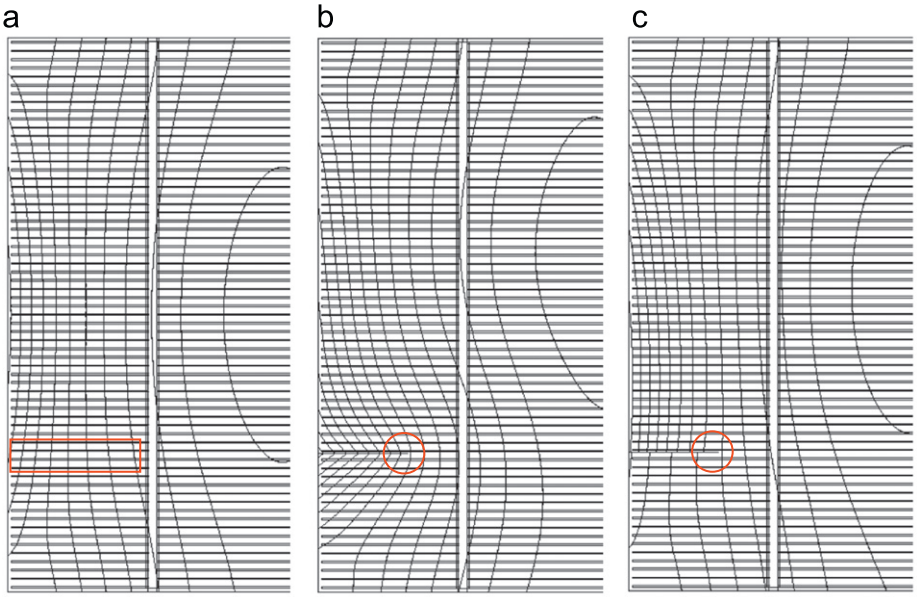

Fig. 2. Zoomed imaged of calculated out-of-plane displacement contours for 25 mm long (a) scratch, (b) surface crack, and (c) through crack initiated at one-quarter periphery off the center of left edge in a polycrystalline silicon solar cell. The marked circular regions are the initiating point of crack extension, and the rectangular is the scratch area. Each contour increment is 266 nm.

thickness direction, and 115,806 elements in the plane of the wafer.

Three kinds of defects were considered. The first is a scratch, which represents a superficial flaw on the surface of solar cell. Scratches were simulated by removing the material occupied within a volume of 25 mm in length, 0.6 mm in width, and 0.01 mm in depth from the cell surface. The second is a surface crack, which we define to be a crack that has propagated through the silicon layer but not through into the aluminum layer. This surface crack was simulated as a vertical planar flaw extending from cell surface and terminating at the underlying Si layer. The third type of crack considered is a through crack, which we define as a crack that penetrates the entire solar cell, from the surface through the Al layer. Fig. 2 shows a comparison of calculated out-of-plane displacement contours for the 25 mm long scratch, surface crack, and through crack initiated at the lower quarter point of the left periphery in a polysilicon solar cell. The contours in the vicinity of the defects are continuous, chevron-shaped, and broken for scratches, surface cracks, and through cracks, respectively. The contour intervals are 0.266 μm similar to one-half wavelength of the DPSS green laser used in the ESPI measurement for out-of-plane displacement.

In through crack modeling we found that the displacement field strongly varies in the vicinity of cracks when the cell model was subjected to heating. The predicted ESPI contours appear broken on both sides of the crack due to a discontinuity in out-of-plane displacement (Fig. 2(c)), suggesting that through cracks in solar cells should be easily detectable during in ESPI inspection. In Fig. 3, we plot vertical displacement along a crack in response to different increases in temperature. Two edge initiated cracks are shown. One is centered at the mid-point of the edge (Fig. 3(a)), falls along one of the symmetry lines of the square-shaped solar cell. The other (Fig. 3(b)) falls off one quarter periphery from the mid-point of the edge and represents a more general through crack. In both cases, vertical displacements of 1–3 μm can be seen. In the centered crack, displacements on both sides of the crack are identical and hence symmetric. In the more general case of off-centered cracks, displacements differ on opposite sides of the crack. Maximum displacements are seen where the crack initiated, and reduced displacements are found near crack tip (Fig. 3(b)). Importantly, the generally asymmetric vertical displacement fields appear to be a distinctive feature of through cracks.

In surface crack models, we assume that crack depth is equal to the Si-layer thickness. Unlike the asymmetric displacement field around through cracks, out-of-plane displacements are always identical on both sides of the crack at a given position along the crack. Fig. 4 shows the out-of-plane displacement with respect to length of the surface cracks for the same boundary condition as shown in Fig. 3. The out-of-plane displacement rises from crack tip to the location of the crack initiation and corresponds to total vertical displacement of 2 μm. For the contour interval of 0.266 μm, this displacement field should produce numerous contours near the crack as shown in Fig. 2(b).

In Fig. 5, we overlay these crack displacement fields with the background displacement field for a defect-free solar cell for 0.4° of heating. First, it is found that in both types of cracks, vertical displacement fields are distinct enough from the background displacement field to be identified by ESPI. Second, it can be seen that surface cracks result in the largest amount of vertical displacement and show symmetric displacement around the crack. Third, the through cracks show intermediate net displacements, but are asymmetric in the displacement field. To assess how diagnostic these displacement fields are, we also examined the deflection angle of contours across a crack as a function of relative penetration depth, which we define as the ratio of crack depth d to layer thickness h (Fig. 6). It is shown in Fig. 6 that below a crack depth ratio d/h <50–60%, there is no contour deflection, when $d/h>60\%$ measurable deflection angles are observed. The contour spacing can be calculated by the crack length divided by the number of contours passing through the crack line. From Fig. 4(a), we estimate the tolerance of measuring crack length to be about 2.65 mm for a 25 mm long centered crack. We consider this the minimum threshold for detection of a crack by this approach.

Finally, an important conclusion of our feasibility test is that small thermal loads generate sufficient deformation to be investigated by ESPI. The ability to monitor deformation using small thermal loads is ideal because the time needed to heat the thin crystalline silicon solar cell is of short duration. These small

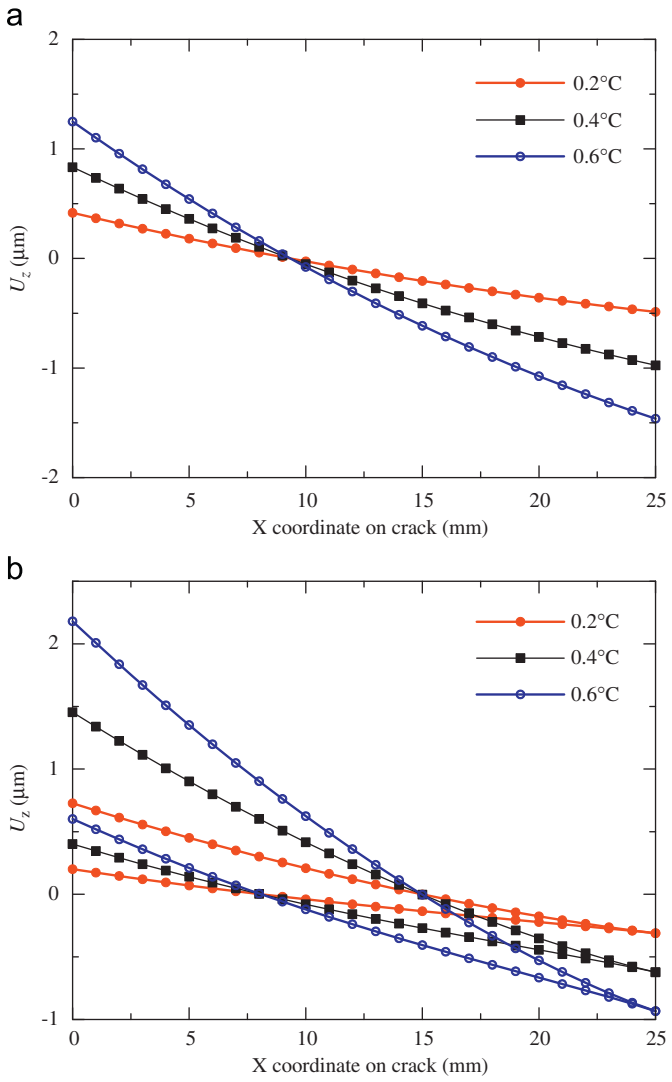

Fig. 3. Out-of-plane displacement field for 25 mm through crack at different ΔT on solar cell model. (a) Crack is centered at the mid-point of the edge. (b) Crack starts from the quarter point of the edge. The coordinate 0 and 25 indicate the crack initiation and tip.

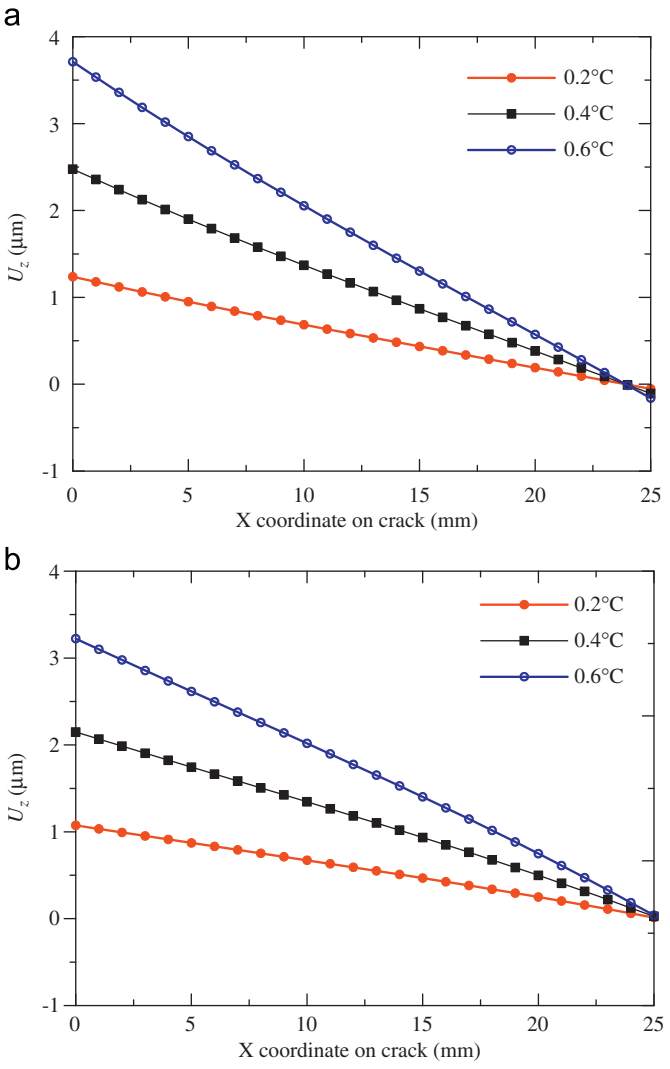

Fig. 4. Out-of-plane displacement field for 25 mm surface crack at different ΔT on solar cell model. (a) Crack is centered at the mid-point of the edge. (b) Crack is initiated at the quarter point of the edge. The coordinate 0 and 25 indicate the crack initiation and tip.

thermal loads do not in themselves cause further cracking or damage to the cell.

3. Experiments

For our test specimens, we used mass-produced crystalline silicon PV cells with dimensions of $156 \times 156 \times 0.2$ mm. We also used single-crystalline silicon solar cells of similar dimensions but with corner reduction up to 15×15 mm. The front surface of the test specimen was coated with a dark blue anti-reflection film (0.08–0.1 μm thick), which was spread to the standard metal contacts. The back surface was screen-printed with a 30–35 μm thick Al paste.

The ESPI was setup as shown in Fig. 7. The specimen was clamped at its four corners. The coherent light source was a DPSS laser with a 532 nm wavelength. The entire specimen surface was illuminated by passing an expanded laser beam through a spatial filter, which revealed deformation in the full-size cell. The reflected beams from the specimen and reference plane crossed each other through the beam splitter and were projected onto a CCD sensor with 2448×2050 pixels. A temperature-controllable planar heater was used to apply a heat flux to the specimen. The heater temperature was measured with J-type thermocouples through a NI-9213 module (National Instruments Corporation). A series of specklegrams for temperature increments were captured by the high resolution CCD camera. The ESPI image was taken from the back of the solar cells because ESPI is more suited for detecting rough rather than smooth surfaces. The image from the camera was controlled by LabVIEW and recorded on a personal computer.

Initial flexural deflection is difficult to fully suppress in single- or polycrystalline silicon solar cells because the thermal expansion coefficients of the screen-printed contacts on the front and back of the cell differ from that of the substrate. Flexural deformation is induced by thermal mismatch in the cell when it is uniformly heated. Speckle images were therefore captured between 30 and 50 °C in increments of 0.2 °C. The speckle interference patterns were determined by subtracting two pictures recorded at different temperatures. The fringe pattern corresponds to a topographic map similar to the out-of-plane displacement contours of the specimen surface. The contour interval is $\lambda/2$ per fringe order [19], where λ is the wavelength of illuminating source. The fringe sensitivity of the current detecting system is 0.266 μm. The ESPI method identifies surface

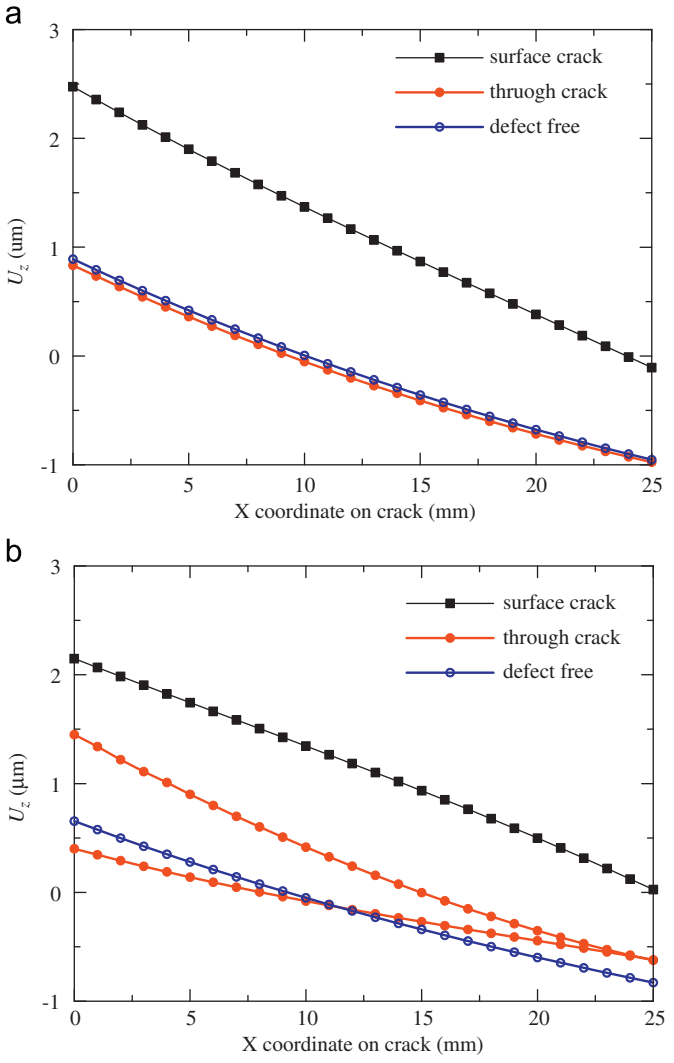

Fig. 5. Comparison of out-of-plane displacement field for 25 mm through crack, surface crack at 0.4° temperature rise on solar cell model. (a) Cracks are centered at the mid-point of the edge. (b) Cracks are initiated at the quarter point of the edge.

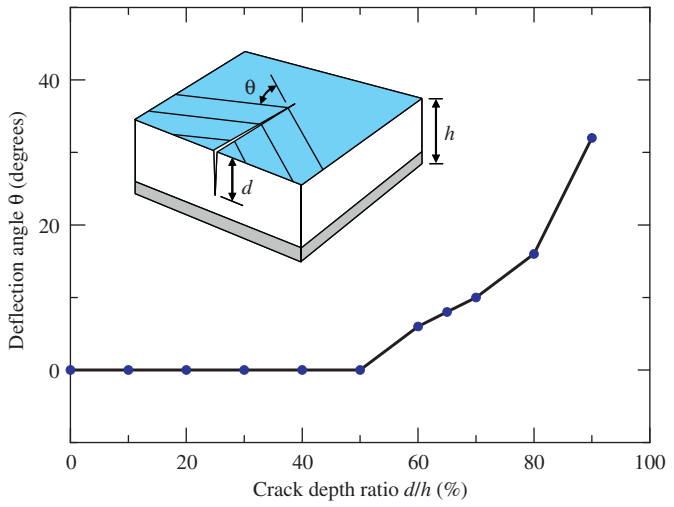

Fig. 6. Deflection angle of the contour across the surface crack with respect to the crack depth ratio. The crack of length 25 mm extends from the middle periphery of the cell.

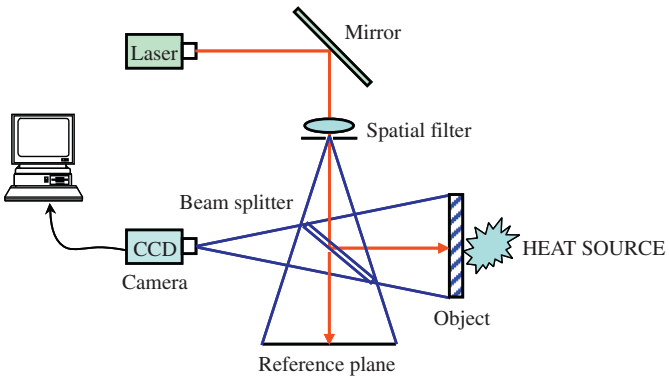

Fig. 7. ESPI configuration for measuring out-of-plane displacement.

deformation by analyzing the fringe pattern of the specimen. The fringe patterns vary for different boundary conditions as shown in our FEM models. Fringe density corresponds to total magnitude of displacement, which depends on the difference in temperature between two recorded images. The larger the temperature rise, the denser the fringe patterns for a fixed contour interval. However, excessively dense fringe patterns must be avoided. A 0.4 °C temperature increase from 32 to 32.4 °C is optimal for recording speckle images since, as shown above, it reveals sufficient fringe densities around cracks but does not further propagate or initiate new cracks.

In order to compare to more traditional methods of assessing the structural integrity of solar cells, we also present EL images even though the EL method cannot quantify the nature of defects in polycrystalline silicon cells. The EL images of all defective and non-defective specimens were acquired with a MT-EL-H1708M EL tester (Scientek Corp., Taiwan). Cracked solar cells excited with 1.5 A current and 3 V were measured at a resolution of 1392 × 1040 pixels. Our EL images, however, represent the mirror image of the ESPI image because the former was taken from the front of the solar cell.

In our experiment, we explored thermally induced displacement fields near cracks starting at the edge of the specimen and extending inward as well as cracks located in the inner area of the specimen. These cracks were pre-formed in the specimens by applying pressure with a small pyramid-shaped diamond indenter attached to a Matsuzawa digital Rockwell-type hardness tester. For reasons already discussed above, most of these pressure-induced cracks generate surface cracks, which terminate at the Al–Si eutectic layer. In order to create through cracks in the solar cells, we used a pencil eraser to apply a light force at the crack tip. This increases the length of cracks, causing them to propagate through the entire PV cell.

4. Results and discussion

Specific interferometric fringe patterns were acquired by first measuring out-of-plane displacement for an undamaged solar cell specimen. Fig. 8(a) shows an out-of-plane ESPI image of an undamaged crystalline silicon solar cell under thermal load. The fringes were dense in the areas near the right and left edges of specimen, indicating greater displacement on the edges than in the central region. The dense fringe pattern with fine spacing in the peripheral regions benefits the inspection of edge cracks. The out-of-plane displacement distribution was also identified by modeling shown in Fig. 8(b), and depicts the contours corresponding to the experimental fringe patterns by ESPI.

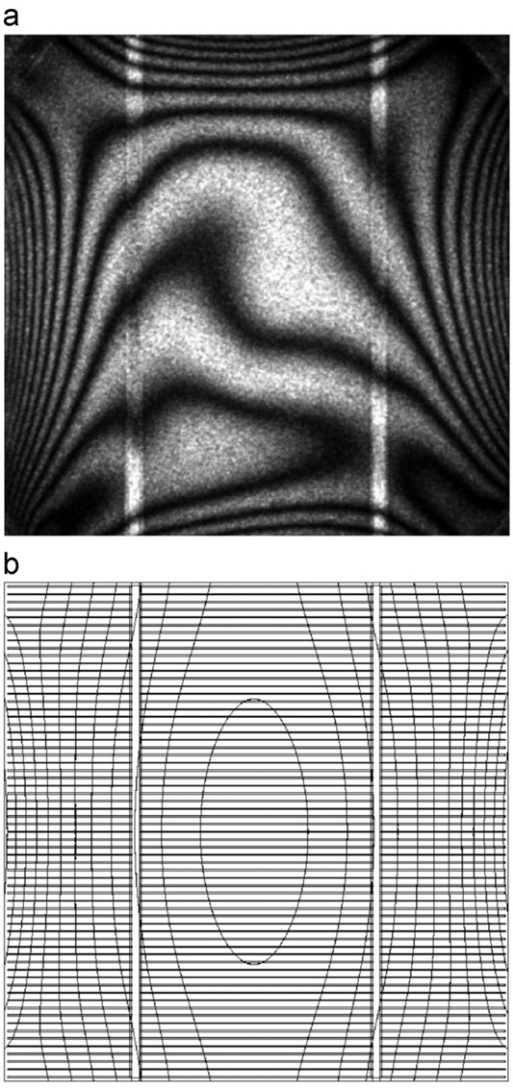

Fig. 8. Out-of-plane displacement of $156 \times 156 \times 0.2$ mm polycrystalline silicon solar cell induced by temperature rise from 32 to 32.4 °C. (a) Speckle fringes due to temperature rise from 32 to 32.4 °C and (b) contour of out-of-plane displacement calculated by FEM.

Fig. 9(a) displays defect patterns from a cracked solar cell acquired by EL imaging. An around 38 mm crack is visible on the edge of the polycrystalline silicon solar cell. Fig. 9(b) shows the ESPI image for the same specimen as shown in Fig. 9(a). As expected, the interferometric fringe patterns as well as the contour distribution by FEM break across the crack line, substantially differing from those in the background defect-free sample shown in Fig. 8(a). Fig. 9(c) shows a simulated contour map of the out-of-plane displacement caused by a through crack in a solar cell with geometry and crack distribution identical to that in the experiment. It can be seen that the contours break around the crack, consistent with our experimental results.

Fig. 10(a) shows an EL image captured from the front surface of a polycrystalline silicon solar cell. The dashed circle indicates a 22 mm long surface crack on the edge. Fig. 10(b) is an ESPI image of the same specimen. The speckle patterns of the cracked solar cell also differ from those of the undamaged specimen shown in Fig. 8(a). The thermally-induced variation of displacement field across the crack surface is discontinuous. Dense interference fringes with chevron shaped patterns are generated near the crack. Fig. 10(c) demonstrates a simulated contour map of the out-of-plane displacement in a polysilicon solar cell with geometry identical to that of the experimental cell with a 22 mm long surface crack. The contours are dense and exhibit abrupt changes in orientation similar to the chevron shaped fringes we observe by ESPI in the vicinity of the crack. Numerical analyses of the displacement jump are thus consistent with the experimental observations. In this ESPI experimental system, cracks shorter than 10 mm were accurately detected, and the observable fringe space depended on the resolution of the CCD camera but was generally about 2 mm.

Cracks artificially made in the central region of the specimens were examined in the same manner. The star-shaped cracks were induced using a square-base pyramid-shaped diamond indenter, which generated cracks radiating from a common point inside the cell. Fig. 11(a) and (b) show the EL and ESPI images of the single crystalline specimen with a 30 mm long star crack, respectively. The center of Fig. 11(b) reveals a set of concentric polygons bounded by closed fringes within the near crack field. The diagonals connecting the opposing vertices indicate the branches of the star-shaped cracks. Fig. 11(c) shows the simulated contour map, again consistent with the experimental result (in these simulations, the crack terminates at the Al–Si eutectic layer).

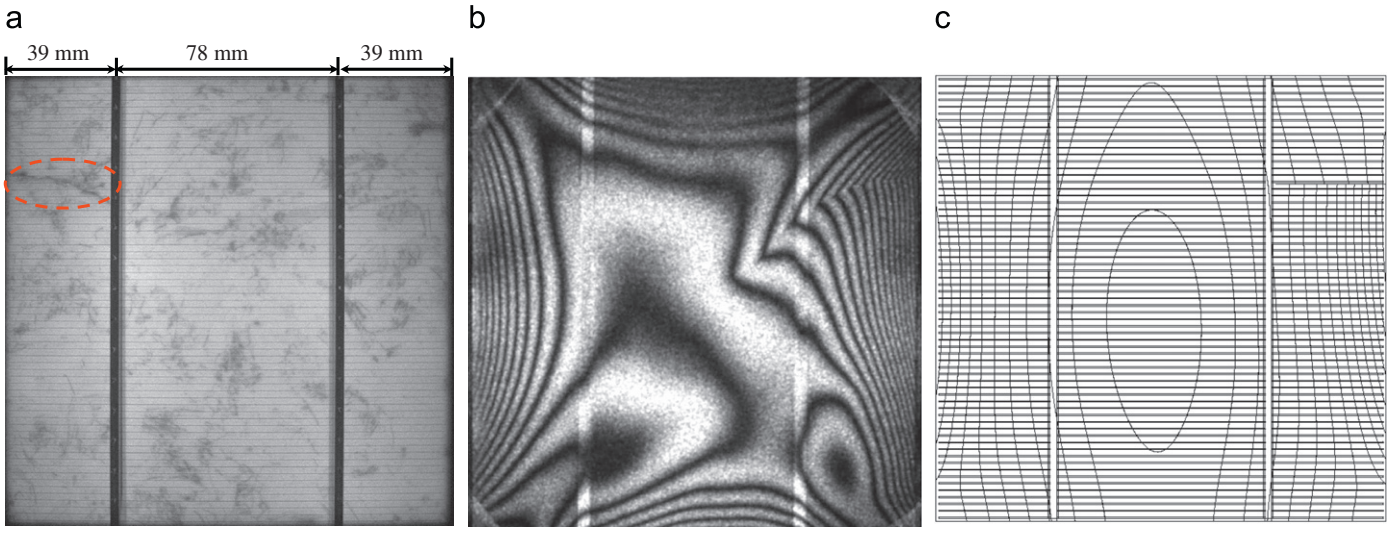

Fig. 9. The $156 \times 156 \times 0.2$ mm polycrystalline silicon solar cell with 39 mm crack on the edge: (a) EL image, (b) ESPI image in temperature range of 32–32.4 °C, and (c) contour map of out-of-plane displacement calculated by FEM. The contour ranges from -2.1 to 2 μm in increments of 0.266 μm.

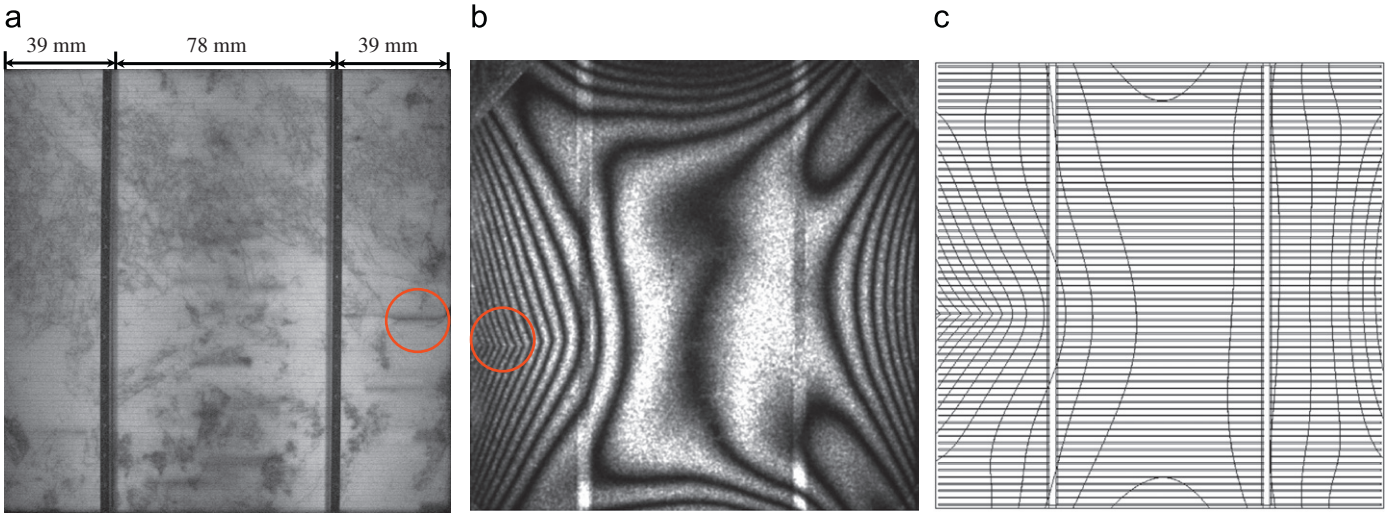

Fig. 10. (a) EL image (front view) for the 156 × 156 × 0.2 mm polycrystalline silicon solar cell with a 22 mm long edge crack, (b) fringe pattern (rear view) caused by temperature rise from 32 to 32.4 °C, and (c) contour of out-of-plane displacement calculated by FEM. The contour ranges from −1.8 to 2.1 μm in increments of 0.266 μm.

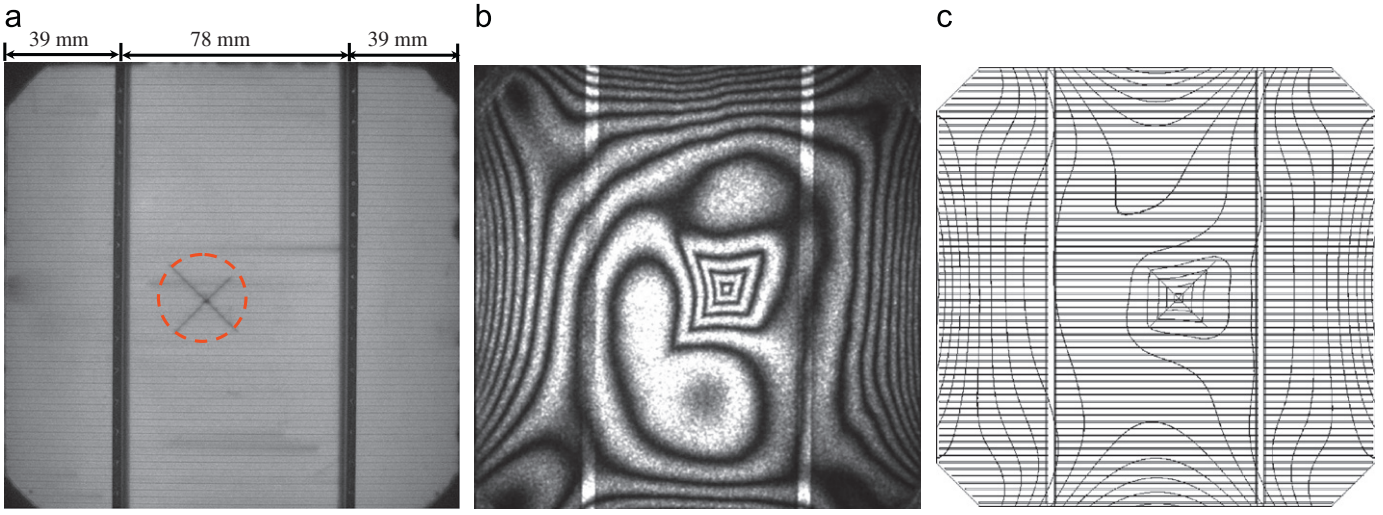

Fig. 11. (a) EL image (front view) and (b) ESPI image (rear view) of a 156 × 156 × 0.2 mm monocrystalline silicon solar cell with a 30 mm long star crack. The fringe pattern is visualized by subtracting of two speckle patterns recorded at 32 and 32.4 °C. (c) Contour of out-of-plane displacement calculated by FEM. The contour ranges from −0.6 to 1.1 μm in increments of 0.266 μm.

5. Conclusion

A rapid, full-field, nondestructive method of inspecting cracks in crystalline silicon PV cells was presented. This method uses ESPI to map out-of-plane deformation (vertical displacement) generated by thermally induced flexural deflection of the specimen. Experimental and numerical results demonstrate that, under similar constraints and temperature rise, defect-free specimens have similar background speckle patterns. However, in flawed specimens, the interference fringes associated with heat-induced deflection clearly differ from those captured in undamaged specimens, particular in the vicinity of cracks. Both experiments and numerical simulations indicate that discontinuous speckle fringes and chevron shaped patterns characterize the near-crack field for both through cracks and surface cracks exceeding 60% of total thickness. In contrast, surface scratches degrade electrical performance but do not substantially change the displacement field under the thermal load. Thus, one advantage of this method is that cracks can be distinguished from surface scratches. Finally, the temperature increase required for inducing moderate speckle fringe density near a crack is less than 0.4 °C, hence, only short duration heating is needed to impart deformations large enough to be detected by ESPI. This method may satisfy the immediate need for rapid quality assessment of PV cells on the manufacturing assembly line.

Acknowledgment

This work was supported by the Hsinchu Science Park Administration, National Science Council of the Republic of China. The authors thank Prof. Cin-Ty Lee of Rice University for valuable comments and discussions on this manuscript.

References

[1] A.W. Blakers, T. Armour, Flexible silicon solar cells, Solar Energy Materials and Solar Cells 93 (2009) 1440–1443.
[2] J.A. Hauch, D. Holland, M.P. Marder, H.L. Swinney, Dynamic fracture in single crystal silicon, Physical Review Letters 82 (19) (1999) 3823–3826.

[3] M.F. Hafiz, T. Kobayashi, Fracture toughness of eutectic Al–Si casting alloy with different microstructural features, Journal of Materials Science 31 (1996) 6195–6200.
[4] I. Chasiotis, S.W. Cho, K. Jonnalagadda, Fracture toughness and subcritical crack growth in polycrystalline silicon, Journal of Applied Mechanics 73 (2006) 714–722.
[5] M.M. Hilali, J.M. Gee, P. Hacke, Bow in screen-printed back-contact industrial silicon solar cells, Solar Energy Materials and Solar Cells 91 (2007) 1228–1233.
[6] T. Fuyuki, H. Kondo, T. Yamazaki, Y. Takahashi, Y. Uraoka, Photographic surveying of minority carrier diffusion length in polycrystalline silicon solar cells by electroluminescence, Applied Physics Letters 86 (2005) 262108.
[7] P. Würfel, T. Trupke, T. Puzzer, E. Schaffer, W. Warta, S.W. Glunz, Diffusion lengths of silicon solar cells from luminescence images, Journal of Applied Physics 101 (2007) 123110.
[8] T. Trupke, R.A. Bardos, M.C. Schubert, W. Warta, Photoluminescence imaging of silicon wafers, Applied Physics Letters 89 (2006) 044107.
[9] M. Kasemann, M.C. Schubert, M. The, M. Köber, M. Hermle, W. Warta, Comparison of luminescence imaging and illuminated lock-in thermography on silicon solar cells, Applied Physics Letters 89 (2006) 224102.
[10] O. Breitenstein, M. Langenkamp, O. Lang, A. Schirrmacher, Shunts due to laser scribing of solar cells evaluated by highly sensitive lock-in thermography, Solar Energy Materials and Solar Cells 65 (2001) 55–62.
[11] W. Dallas, O. Polupan, S. Ostapenko, Resonance ultrasonic vibrations for crack detection in photovoltaic silicon wafers, Measurement Science and Technology 18 (2007) 852–858.
[12] K. Nassim, L. Joannes, A. Cornet, S. Dilhaire, E. Schaub, W. Claeys, Thermomechanical deformation imaging of power devices by electronic speckle pattern interferometry (ESPI), Microelectronics Reliability 38 (1998) 1341–1345.
[13] E. Hack, R. Brönnimann, Electronic speckle pattern interferometry deformation measurement on lightweight structures under thermal load, Optics and Lasers in Engineering 31 (1999) 213–222.
[14] E.A. Zarate, E.G. Custodio, C.G. Treviño-Palacios, R. Rodríguez-Vera, H.J. Puga-Soberanes, Defect detection in metals using electronic speckle pattern interferometry, Solar Energy Materials and Solar Cells 88 (2005) 217–225.
[15] A.T. Zehnder, M.J. Viz, Fracture mechanics of thin plates and shells under combined membrane, bending and twisting loads, Applied Mechanics Reviews 58 (2005) 37–48.
[16] V.A. Popovich, M. Janssen, I.M. Richardson, T. van Amstel, I.J. Bennett, Microstructure and mechanical properties of aluminum back contact layers, Solar Energy Materials and Solar Cells 95 (2011) 93–96.
[17] M.A. Hopcrot, W.D. Nix, T.W. Kenny, What is the Young's modulus of silicon? Journal of Microelectromechanical Systems 19 (2) (2010) 229–238.
[18] C.S. Oh, W.N. Sharpe Jr., Techniques for measuring thermal expansion and creep of polysilicon, Sensors and Actuators A 112 (2004) 66–73.
[19] R.S. Sirohi, F.S. Chau, Optical measurement techniques and applications, Artech House, Inc., 1997, pp. 148–162.